A SEPIC-BUCK TOPOLOGY FOR REMOTELY PILOTED AIRCRAFT SYSTEMS BATTERY CHARGER

Rafael H. Eckstein[1], Eduardo V. de Souza[1], Maikel F. Menke[2], Telles B. Lazzarin[1]
[1]Federal University of Santa Catarina (UFSC), Florianópolis-SC, Brazil
[2]Federal Institute of Santa Catarina (IFSC), Florianópolis-SC, Brazil
e-mail: rafael.eckstein@ifsc.edu.br, eduardovalmir@gmail.com, maikel.menke@ifsc.edu.br, telles@inep.ufsc.br

***Abstract* – The use of remotely piloted aircraft systems (RPAS) is already a reality in applications such as geographic mapping, surveillance, digital marketing, delivery, agriculture, infrastructure inspection, and others. Most of these aircraft are purely electric, being the only source of energy, packs of ion-lithium or lithium polymer batteries. These battery packs are conceived by the association of a different number of cells, usually ranging from three cells (3S) to twelve cells (12S). However, universal battery chargers for this range are not consolidated yet due to the recent emergence of the use of RPAS for different applications. To overcome this drawback, this paper introduces a topology to charge a wide range of low voltage battery packs (3S-12S) for RPAS. The circuit is composed of two power converters, one of them is a DCM SEPIC PFC rectifier and another is a dc-dc Buck converter. The system is design for 400 W of rated power and the proposed solution is suggested to charge battery packs from 3S to 12S.**

***Keywords* – Battery charger, dc-dc Buck converter, drone, RPAS, SEPIC PFC rectifier.**

NOMENCLATURE

V_b	Battery voltage.
V_{dc}	Dc-link voltage.
V_{bref}	Battery voltage control reference.
V_g	Electrical grid voltage.
V_p	Electrical grid peak voltage.
t_1	Time the SEPIC switch is on.
t_2	Time the SEPIC diode is on.
T_s	Switching period.
f_s	Switching frequency.
D_{sepic}	SEPIC static gain.
$D_{sepic.crit}$	SEPIC static gain in critical condution mode.
D_s	SEPIC diode.
S_s	SEPIC switch.
L_s	SEPIC inductor.
L_p	SEPIC inductor.
L_{eq}	SEPIC equivalent inductor.
C_s	SEPIC coupled capacitor.
C_{dc}	Dc-link capacitor.
R_o	SEPIC resistive load.
d_b	Duty cycle of the Buck converter.
L_B	Buck inductor.
Δi_{L_B}	Buck inductor current ripple.
D_{buck}	Buck static gain.
D_B	Buck diode.
S_B	Buck switch.
C_B	Buck output capacitor.
R_B	Buck resistive load.
I_b	Buck output current.
I_{bref}	Charge current reference.
P_o	Output power.

Manuscript received 10/02/2021; first revision 11/08/2021; accepted for publication 03/22/2022, by recommendation of Editor Marcelo L Heldwein. http://dx.doi.org/10.18618/REP.2022.1.0039.

I. INTRODUCTION

The use of remotely piloted aircraft systems (RPAS) or, as more popularly known as drones, has been expanding [1], especially in the areas of monitoring, mapping, agriculture [2]–[4] and delivery. Usually, such aircraft may have configurations with four (quadcopter), six (hexacopter), or eight (octacopter) rotors, and it can be purely electric, in which only batteries provide power to the system, or hybrid, with a combustion engine, supercapacitor, or fuel cell [5], [6] with a battery pack in parallel, frequently for back-up in case of a failure in the main power source.

Airscraft systems are named as purely electric RPAS, when they depend exclusively on the battery pack. Usually, they have a low flight autonomy compared to hybrid drones. On the other hand, they can be lighter, have less vibrations, and, additionally, they do not contribute to local pollution [7].

The battery packs used in RPAS are mostly made up of lithium-polymer (LiPo), which consist of a lithium-ion battery with a polymeric material (as electrolyte) and presents a varying voltage level ranging from 3S (three cells connected in series) to 12S. The nominal voltage of each cell may change according to the battery chemistry, but the most common is 3.7 V, the minimal voltage should not be less than 3.0 V and the maximum is around 4.2 V. So, a 3S battery pack, would have a minimum, rated and maximum voltage of 9.0 V, 11.1 V and 12.6 V, respectively. Table I presents some commercial battery packs manufactured for RPAS.

The most commonly used charging method in lithium-ion battery packs is CC-CV (constant current-constant voltage) [8]–[11], in which initially a constant current is applied to the terminals of the storage system until it reaches a predetermined maximum voltage level. Then, the constant voltage stage begins, and the voltage in the battery terminals remains regulated while the current decreases naturally up to a minimum value, usually below 10% of the rated current [12], when the recharge is considered full.

The charge rate, given by the constant current intensity applied in the firste stage of charging process, is determined

TABLE I
Commercial Battery Pack

Manufact.	Capacity (Ah)	N° of cells	Voltage (V)
Zop Power	4.0	3	11.1
Gens Ace	4.5	3	11.1
Traxxas	6.4	3	11.1
Turnigy	5.0	6	22.2
Ovonic	5.5	6	22.2
Yowoo	10.0	6	22.2
Tattu	5.0	12	44.4
Tattu	10.0	12	44.4

concerning the battery capacity. Manufacturers generally specify a charge rate of 1C, so a battery pack like the Ovonic 22.2 V/5.5 Ah should be charged with a constant current of 5.5 A until it reaches the maximum battery pack voltage.

Analyzing Table I, it is perceived the variety of voltage levels and capacity of the battery packs used in RPAS, so it is necessary a versatile charger, capable of operating, optimized, over a wide operation range. Few commercially available chargers include all configurations (3S to 12S) and it is difficult to get performance data throughout the whole voltage range. In addition, studies seeking the optimization of static converters used in battery chargers are limited. Typically, this analysis is performed for a range of chargers in the tens of kW range. [13]–[16]. As a result, a gap exists in the development of high-performance chargers for applications requiring a few hundred Watts or less.

Typically off-board chargers feature two stages of power processing, a front-end ac-dc power factor correction (PFC) stage, and a dc-dc converter that monitors and performs battery pack charging (Figure 1). PFC Boost-type rectifiers are commonly used in high-power battery pack chargers used in electric vehicles, due to their simplicity, great performance [15], [16] and the need to adequate the voltage level to charge the battery banks, which have nominal voltage between 150-450 V [17], normally above the electrical grid. On the other hand, for few hundred of watts, PFC rectifiers based on Buck-Boost, Zeta, Cuk and SEPIC converters have been employed also outcoming with a high perfomance. Furthermore, the constant input current of the SEPIC PFC rectifier operating in discontinuous conduction mode reduces the demand for an input filter.

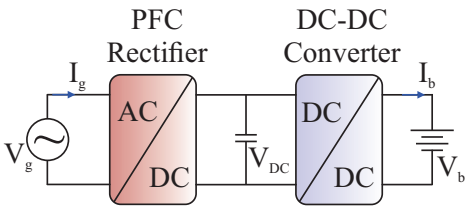

Fig. 1. Typical two-stage charger topology.

The dc-dc converters are mostly composed of full-bridge ZVS topologies or Resonant LLC [16], when galvanic insulation is required. Buck-type converters are also employed in the second load stage [18], when galvanic insulation is not required. There is no such need for isolation in the SAE J1772 regulations for EV safety and in lower power it can be not used [19]. Despite the fact that there are several studies on battery chargers in the literature, few studies on wide range low voltage systems are available.

Therefore, to overcome this drawback, this work presents an optimized charger for LiPo battery packs with a rated voltage level between 11.1 V to 44.4 V and 400 W of rated power. The system, presented in Figure 2, consists of a SEPIC PFC rectifier operating in discontinuous conduction mode (DCM) and a dc-dc Buck converter for charging, the analysis of each one is undertaken in the following section.

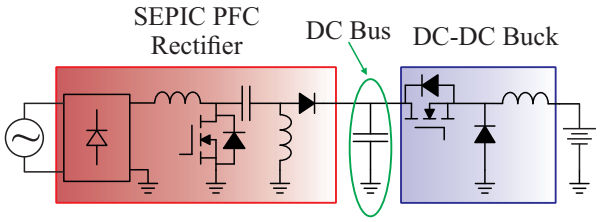

Fig. 2. Proposed system.

II. PROPOSED SYSTEM

The proposed topology consists of a SEPIC PFC rectifier with a diode bridge and a dc-dc Buck converter connected to the terminals of the battery pack. As shown in Figure 3, the SEPIC PFC rectifier operates in DCM and it has three stages of operation.

- 1st step (0 - t_1) - During this step the switch (S_s) is on, conducting the current, the diode (D_s) is blocked and reversely polarized with a voltage equal to the dc-bus, V_{dc}. Inductors (L_s and L_p) store the energy from the power supply, V_g and capacitor, C_s, respectively, and the currents increases linearly until they reach their peak value, at t_1 , when the switch is turned off ends the first operation stage (Figure 3.a).
- 2nd step (t_1 - t_2) - This step starts at t_1, when the switch is turned off and subjected to a voltage equal to the sum of the input and output voltage. The inductors are demagnetized and their currents, which are driven by diode, D_s, decrease linearly until t_2, when they cancel each other, interrupting the current in the diode and finishing this stage. To ensure proper operation in DCM, t_2 must be less than the total period, T_s. Figure 3.b displays the equivalent circuit of the rectifier at this step of operation.
- 3rd step (t_2 - T_s) - In the last step, both the switch and diode are not conducting, the currents of the inductors L_s and L_p are constant and equal, with opposite direction to each other. During this stage the load is fed by the bus, V_{dc}. This step (Figure 3.c) ends when the switch is turned on, and the first step is repeated once more.

The rectifier's operational steps are identical for the two half cycles of the electrical grid voltage, with the exception of the rectifier bridge pair of diodes that will conduct the current from the input source.

The choice for the SEPIC converter to operate in the rectifier stage was due to the following advantages: (i) operates as a step-down converter; (ii) current characteristic at the input, facilitating the correction of the power factor;

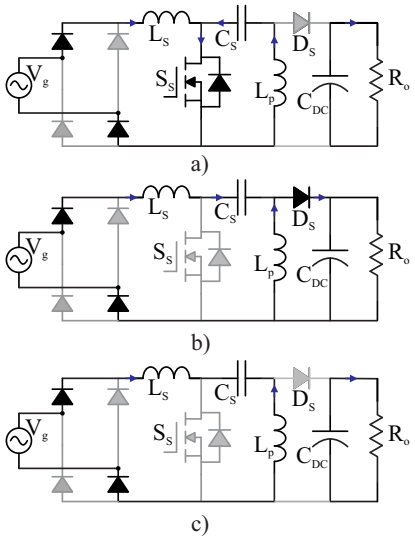

Fig. 3. DCM SEPIC PFC rectifier operations steps during a semi cycle of the input voltage.

(iii) when operating in DCM, it behaves like a resistive load to the input AC source, therefore, the input current follows the waveform of the voltage ensuring a power factor close to the unit without the need of a current sensor; (iv) it has only one active switch, which does not require an isolated driver; (v) possibility of galvanic insulation between input and output by replacing the inductor L_p for a transformer [20].

The dc-dc Buck converter operates in continuous conduction mode, the steps of operation, as well as the equivalent circuits, are described below and presented in Figure 4, respectively.

- 1st Step (0 - d_bT_s) - In this step the switch is conducting. The V_{dc} bus provides power to the load and magnetizes the inductor, L_B. The diode, D_B, is blocked in this step and reversely polarized by a voltage level equal to the V_{dc} bus. Figure 4.a shows the equivalent circuit of the converter for this period.

- 2nd Step (d_bT_s - T_s) - The second step starts when the switch is turned off. The energy stored in the inductor is transferred to the load with the freewheeling diode, D_B. At this stage, the current in the inductor decreases linearly. The equivalent circuit of the dc-dc Buck converter operating in the second step is shown in Figure 4.b.

The Buck converter has been selected to operate in the dc-dc stage because it has certain characteristics, such as: (i) output current characteristic; (ii) step-down converter, required for charging battery packs with few cells connected in series; (iii) presents only one switch, which is positioned in the direct path between the bus and the load, and it can interrupt the current sent to the battery in case of system shutdown. (iv) possibility to be used in an interleaving connection to reduce the ripple of the output current and to increase the rated power [21].

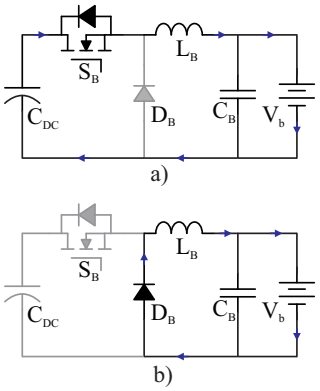

Fig. 4. dc-dc Buck converter operations steps.

III. DESIGN, OPERATION AND CONTROL OF THE SYSTEM

The proposed system presents two stages, the SEPIC PFC rectifier, which performs the correction of the power factor and regulates the V_{dc} bus voltage and the dc-dc Buck converter, responsible for the battery recharge, employing the CC-CV method. The topology purposes is to charge a wide variety of low voltage batteries with different capacity, which results in a wide range of output power.

In this section is discussed the metodology to choose the magnetic elements, the most adequate dc-link voltage level for a given output power, the initialization of the entire system, and the used control technique.

A. Design of the Converters

Since the system aim is to charge several types of battery banks, evaluating the operational boundary points is required in order to design the components. In addition to this, as it is a system with different battery models with several levels of voltage and current, some components have maximum inductance and capacitance requirements at one point, but they were assembled or specified to satisfy maximum current and voltage generated at another point. However, such an approach causes the system to perform suboptimally for some operation points but close to optimal considering the overall operation range..

The dependecy on the output voltage, V_{dc}, and ripple current may be observed in the design of the SEPIC PFC rectifier's input inductor, L_s, provided by [20] and depicted in (1). In order to maintain a minimum duty cycle of 0.3 in the Buck converter, the maximum dc-bus voltage set for the magnetic component specification was three times the battery bank voltage. With this specified, the critical point for the inductor L_s occurs at the lowest power with the least amount of current ripple. It is noteworthy that for the construction of the inductor the maximum current point was used for the specification of the conductor, because the component have to withstand winding losses for all operation curve, even though this is not the maximum inductance point.

$$L_s = \frac{(V_p \frac{V_{dc}}{V_{dc}+V_p})}{\Delta i_{L_s} f_s}. \tag{1}$$

The L_p inductor design was subjected to a similar study.

According to [20], the conduction relationship, k_a, is defined for the SEPIC PFC rectifier to operate on the MDC, which is given by:

$$k_a = \frac{2L_{eq}P_o f_s}{V_{dc}^2} \tag{2}$$

or

$$k_a = \frac{1}{2(M+1)^2} \tag{3}$$

where

$$L_{eq} = \frac{L_s L_p}{L_s + L_p} \tag{4}$$

and

$$M = \frac{V_{dc}}{V_p}. \tag{5}$$

The equation for the inductance L_p is obtained isolating the equivalent inductance, Leq, and substituting equation (3) in (2).

$$L_p = \frac{L_s V_{dc}}{4(M+1)^2 P_o f_s + V_{dc}}. \tag{6}$$

The Buck converter inductor is designed using the same criteria as previously provided and it may be characterized as follows:

$$L_B = \frac{(V_{dc} - V_b) D_{buck}}{\Delta i_{L_B} f_s}. \tag{7}$$

In order to ensure a charge current with low ripple, the critical point for inductor L_B is defined for a maximum current of 10 A in order not to exceed the established rated power, which will only be processed in batteries with a voltage level below 12S.

B. The DC-link Voltage Definition and System Initialization

The static gain of the DCM SEPIC PFC rectifier is given by [20]:

$$D_{sepic}^2 = \frac{V_{dc}^2}{V_g^2} \frac{2L_{eq} f_s}{R_o}. \tag{8}$$

The static gain of the rectifier in critical conduction mode is set to [20]:

$$D_{sepic.crit} = \frac{M}{M+1}. \tag{9}$$

The duty cycle of the SEPIC PFC rectifier in the DCM must be lower than the critical, and assuming that the power available on the rectifier's output is the same as that delivered to the battery, a relation between the output power and the dc-bus voltage level can be found and it is given by:

$$P_o(V_{dc}) = \frac{V_{dc}^2}{4L_{eq}(M+1)^2 f_s}. \tag{10}$$

Equation (10) behavior is displayed in Figure 5.

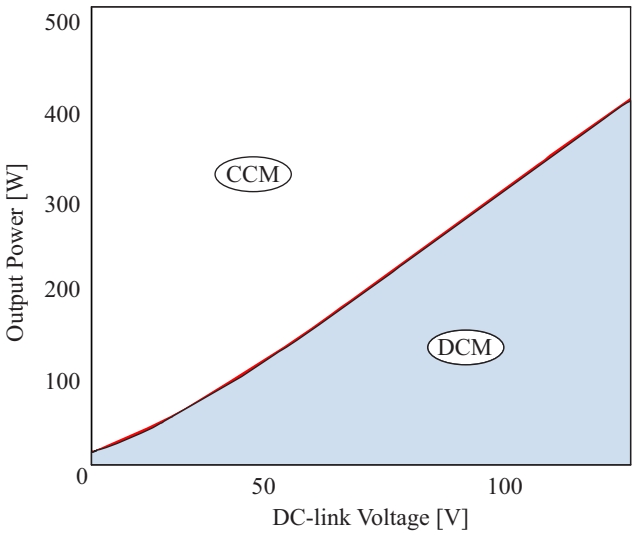

Fig. 5. Relationship between output power and dc bus voltage for DCM mode.

As a result, the dc-bus voltage reference is established based on the power required to charge the battery, to ensure the rectifier operates in discontinuous conduction mode. In addition, the reference value needs to be higher than the battery voltage, to dc-dc Buck converters operates satisfactorily.

The main components of the dc-dc Buck converter power losses are the switch, diode and the inductor losses [22]. A survey of the efficiency of the converter in relation to the input voltage (dc-link voltage), V_{dc}, was carried out.

The losses in the diode, D_B, have a large impact on the voltage and power levels of the system, therefore the dc-dc Buck converter has a higher efficiency at voltage levels at the input close to the output, which needs a high duty cycle.

For a battery bank of the same voltage level but larger capacity, the losses in the switch and in the inductor, as they are directly proportional to the square of the output current, are more prominent, imposing a reduction in the duty cycle and an increase in the voltage of bus V_{dc}. However, when compared to Figure 5, the optimal voltage level determined by the losses calculation is lower than the minimum required by the SEPIC PFC rectifier to function in the discontinuous conduction mode.

Table II presents the optimal voltage levels to the dc-dc Buck converter operation as well as the minimum required by the DCM SEPIC PFC rectifier at various operating points.

In this manner, the system choose the minimum dc-bus voltage, that attends all the criteria, to guarantee the correct rectifier conduction mode and proper static gain for the second stage dc-dc converter.

With the V_{DCref} set, the system begins charging the dc-bus capacitor C_{dc} until the voltage level on the bus reaches the reference value, at which point the SEPIC PFC rectifier and the dc-dc Buck converter are enabled and the first step of the

TABLE II
Controllers Parameters

Battery	Optimum Buck	DCM Minimum
11.1 V/4.0 Ah	12.0 V	28.27 V
11.1 V/6.4 Ah	15.0 V	37.3 V
22.2 V/5.5 Ah	25.0 V	52.32 V
22.2 V/10.0 Ah	30.0 V	78.5 V
44.4 V/10.0 Ah	55 V	135 V

charging method begins, injecting a constant current into the battery terminals.

C. System Control

When operating in DCM, associated with a rectifier bridge, the SEPIC PFC rectifier requires only one voltage control loop to provide power factor correction and a constant voltage level on the bus [23], thus not requiring current sensors. The block diagram of the control loop is shown in Figure 6.a.

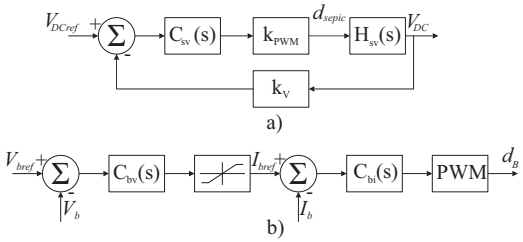

Fig. 6. Control block diagrams.

For a variable output power, the transfer function of the SEPIC PFC rectifier plant model is given by [24]:

$$HGvs(s) = \frac{K_{VD}}{R_o C_{dc} s + 1 + K_{VD}\frac{D_{sepic.crit}}{2V_{dc}}} \tag{11}$$

where:

$$K_{VD} = \frac{V_p^2 D_{sepic.crit} R_o}{V_{dc} L_{eq} f_s}. \tag{12}$$

The system transfer function obtained presents a first-order behavior with a high time constant [20], therefore, a proportional controller would be adequate to regulate the voltage when the converter is subjected to load fluctuations, albeit with an associated inaccuracy. To avoid errors in the steady state, an integral proportional controller is chosen to regulate the rectifier's output voltage.

The control system of the dc-dc Buck converter features two loops. One outer voltage loop and one inner current loop. At the beginning of the charge, the battery pack voltage is less than the maximum reference voltage (maximum voltage of the battery pack), this error when compensated by an integral proportional controller is saturated at the capacity value of the battery, setting the reference current to the charge current control.

When the battery pack voltage approaches the voltage reference value, the output of the voltage controller is no longer saturated and the load current reference decreases until it reaches the minimum, predetermined value, finishing the charge. Figure 6.b shows the two control loops used in the dc-dc Buck converter.

The current and voltage transfer functions used to control the dc-dc Buck converter, is given by, respectively:

$$H_{i_B}(s) = V_{dc}\frac{C_B R_B s + 1}{C_B L_B R_B s^2 + L_B s + R_B} \tag{13}$$

$$H_{v_B}(s) = \frac{V_{dc}}{L_B C_B s^2 + \frac{L_B}{R_B} s + 1}. \tag{14}$$

Integral proportional controllers were also used to control both loops of the dc-dc Buck converter. However, for the proper functioning of the two control loops it is necessary to guarantee the decoupling between them. For this to occur, the current loop (internal) must operate with a higher frequency than the voltage loop (external).

Dynamic tests from the proposed control are depicted in Figures 7 and 8. They illustrate responses of the bus voltage and output current when steps on the dc bus reference and on the load are applied. Firstly, the dc voltage reference (V_{DCref}) is increased by 10% at 0.3 s and thus the bus voltage follows the reference, as shown in Figure 7. In a second test, the current battery reference is increased from 5.0 A to 5.5 A at 0.3 s, as seen in Figure 8. The Buck output current (I_b) follows the reference and the SEPIC bus voltage control loop takes about 100 ms to reject this disturbance. Table III presents the parameters of the controllers used in the proposed system.

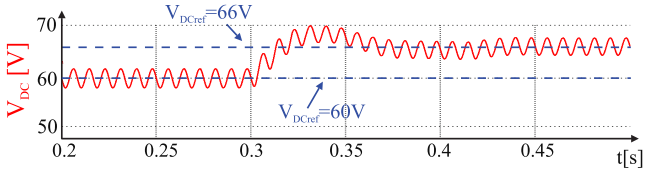

Fig. 7. Step response of the V_{DC} voltage control loop.

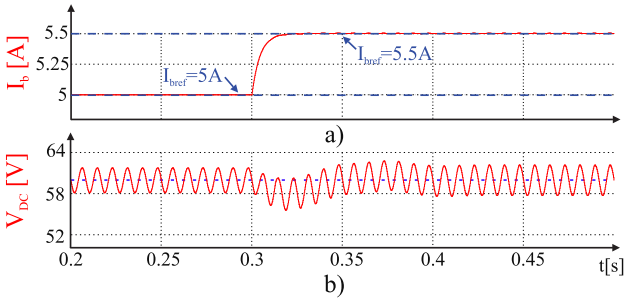

Fig. 8. a) Step response of the dc-dc Buck output current control loop. b) The disturbance rejection of the dc-link voltage control loop.

TABLE III
Controllers Parameters

Parameter	Value
SEPIC - Proportional Gain	1.5
SEPIC - Time constant	2.7 ms
Buck - Proport. Gain (Voltage Loop)	0.0001
Buck - Time constant (Voltage Loop)	1.4 ms
Buck - Proport. Gain (Current Loop)	0.24
Buck - Time constant (Current Loop)	50 μs

IV. SIMULATION AND EXPERIMENTAL RESULTS

The proposed system was simulated and implemented, a picture of the prototype is presented in Figure 9 and Table IV lists the capacitors and inductors that were employed. The charger has been tested with a resistive load emulating critical and intermediate operating points, equivalent to four different battery packs in a 127 V electrical grid. It should be highlighted that these experiments are only the commencement of the research, and that the study will be expanded and tested using genuine Lipo batteries in the future.

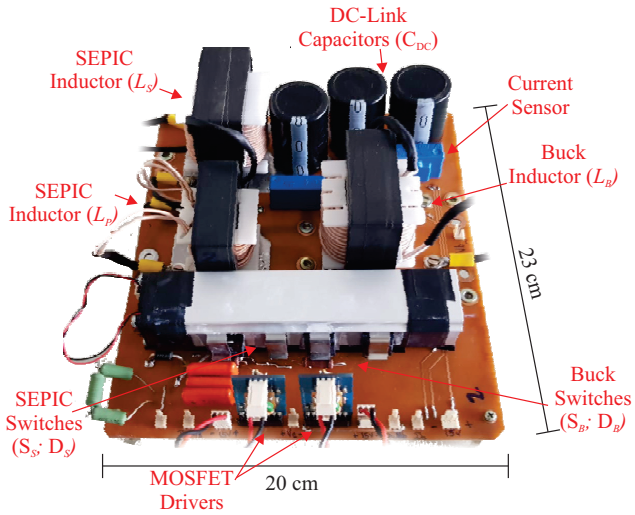

Fig. 9. Built prototype.

TABLE IV
Components Specification

Component	Value
SEPIC Inductor (L_sS)	630 μH
SEPIC Inductor (L_p)	71 μH
SEPIC Capacitor (C_s)	1.5 μF
Dc-Link Capacitor (C_{dc})	1.4 mF
Buck Inductor (L_B)	0.55 mH

In all four tested points the system has started smoothly, initially charging the capacitor, C_{dc}, until the voltage reached the reference value, after which the rectifier and dc-dc Buck converter began to operate, managing the dc-bus voltage and charge current.

The first point of operation consists of a three cells connected in series, with a rated voltage of 11.1 V and 3.8 Ah of capacity. Figure 10 shows the current and voltage at the output of the dc-dc Buck converter and the dc-bus, V_{dc}.

The second point emulates a 3S battery with a capacity of 4.5 Ah. With such defined parameters, the dc-bus reference voltage and the charging reference current are defined. Figure 11.a shows the output voltage and current waveforms of the dc-dc Buck converter and the bus voltage, V_{dc}. The voltage and current of the input source are displayed in Figure 11.b. At this operating point, the power factor and THD were 0.985 and 4.28 percent, respectively. These results were acquired using the MSO 4034 mixed signal oscilloscope.

It is also worth noticing the variation in bus voltage between two batteries with the same number of cells in series but

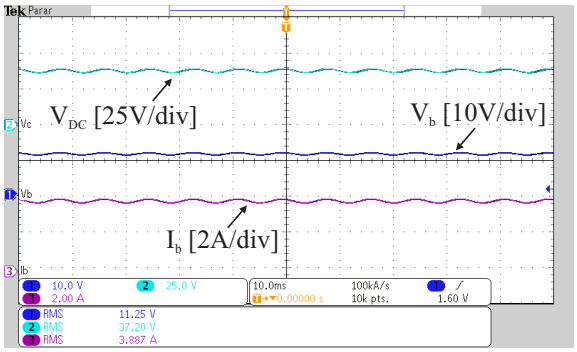

Fig. 10. Waveforms of output voltage and current and dc-bus voltage during a charging emulation of a 3S/3.8 Ah battery bank.

differing capacity. In the second point, because it is a larger bank, the output power is higher, and therefore the bus reference voltage level, according to Figure 5, must be higher.

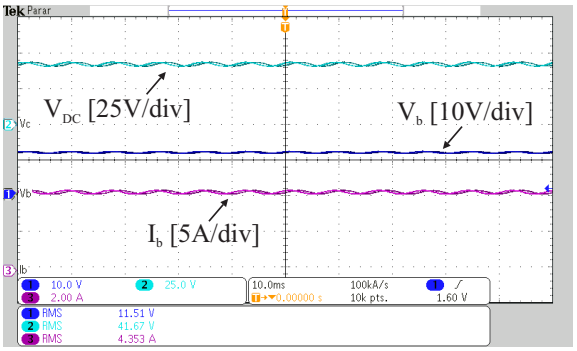

a)

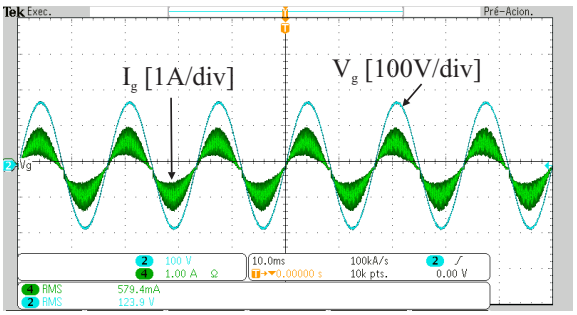

b)

Fig. 11. (a) Waveforms of output voltage and current and dc-bus voltage during a charging emulation of a 3S/4.5 Ah battery bank. (b) Waveforms of electrical grid voltage and current.

The third point tested consider a battery pack with six cells connected in series, with a nominal voltage of 22.2 V, and a capacity of 5.5 Ah. Figure 12 shows the current and voltage at the emulated battery pack terminals, the dc-bus voltage and the SEPIC inductor, L_s, current are displayed as well.

Again, it is possible to see that with the increase in the power processed by the system, the value of the V_{dc} bus voltage also increases, ensuring that the rectifier always operates in DCM.

The last test was perfomed considering a battery pack with twelve cells in series, a nominal voltage of 44.4 V, and a capacity of 8.5 Ah. Figure 13.a shows the current and voltage at the emulated battery pack terminals, as well as the dc-bus voltage and the SEPIC inductor, L_s, current. It is worth

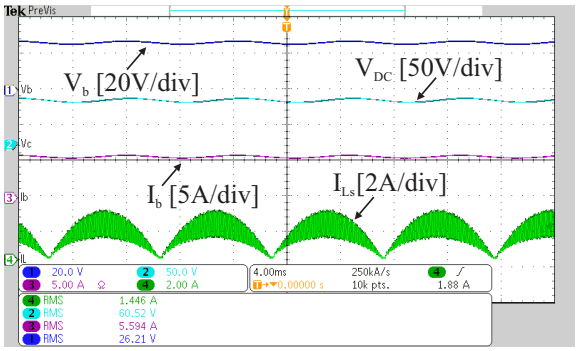

Fig. 12. Waveforms of output voltage and current, as well as the dc-bus voltage and SEPIC inductor current under a charging emulation of a 6S/3.8 Ah battery bank.

noticing that the voltage level at the dc-dc Buck converter's output is lower than the nominal value of 44.4 V or even the maximum value of 50.4 V (4.2 V per cell), emulating a charge in the constant current stage on a low state-of-charge battery. The voltage and current of the electrical grid are shown in Figure 13.b. Through MSO 4034 mixed signal oscilloscope, the THD and power factor obtained when the system operates at rated power were 2.07% and 0.990, respectively.

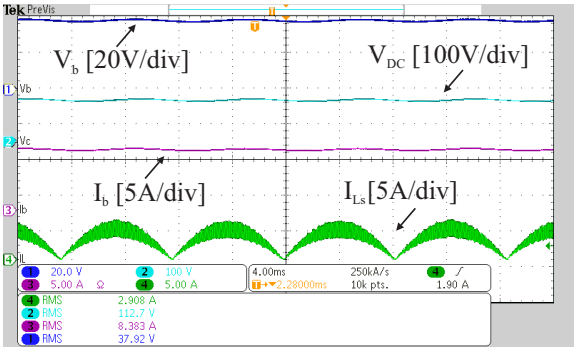

a)

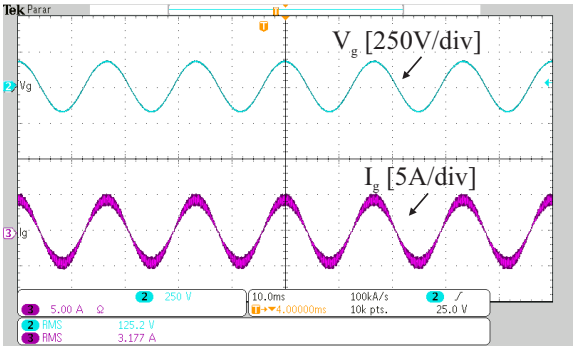

b)

Fig. 13. (a) Waveforms of output voltage and current and dc-bus voltage during a charging emulation of a 12S/8.5 Ah battery bank. (b) Waveforms of electrical grid voltage and current.

The losses in the semiconductors and magnetic parts of the system were also examined at this test point. A pie chart depicting the percentages of losses for each component is shown in Figure 14.

In order to compare the findings achieved in simulation and experimental tests, Figures 15 and 16 describe the behavior of the simulated system charging a 12S/8.5 Ah battery bank.

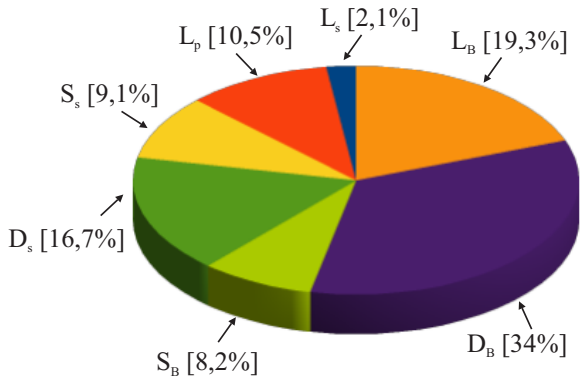

Fig. 14. The percentage of experimental losses in semiconductor elements and magnetic elements when charging a 12S/8.5 Ah battery bank.

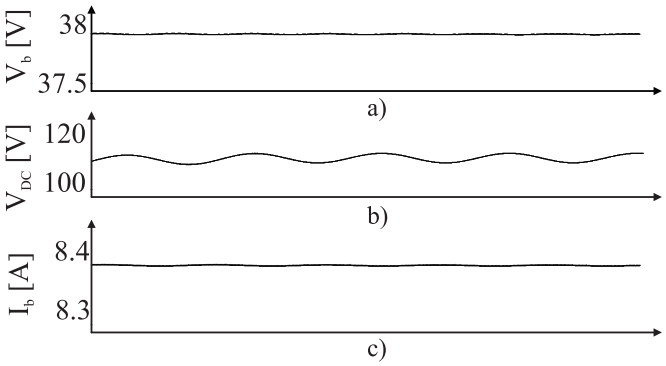

Fig. 15. Simulation result of the system charging a 12S/8.5 Ah battery. (a) Output voltage waveform. (b) Dc-bus voltage waveform. (c) charging current waveform.

It should be noted that the system works as designed by comparing the findings produced in the experiments with the simulation. In both cases, the battery current was set to charge the battery bank at a rate of 1C. As predicted, the bus voltage has a steady mean value equal to the reference with a ripple at 120 Hz. Finally, the current and voltage from the electrical grid have a power factor close to unity, with a value of 0.998 in the simulation and 0.990 in the experiment.

According to all the test that were made, the system performed satisfactorily for the three distinct voltage levels of battery packs, achieving the goal of charging a large number of packs of various levels and capacities. In all testing, the system displayed a power factor close to the unit and a steady dc-bus voltage level, as specified.

V. CONCLUSIONS

This work presented the study and experimental results of an electronic system to charge battery packs of remotely piloted aircraft systems. The proposed system is capable of charging battery packs consisting of three lithium polymer cells (3S - 11.1 V) to packs with twelve cells connected in series (12S - 44.4 V), covering a vast amount of packs currently used in drones. The charger also performed satisfactorily in power factor correction, maintaining the current in phase with the voltage of the electrical network at the different operating points.

The prototype also features a starting system, in which the

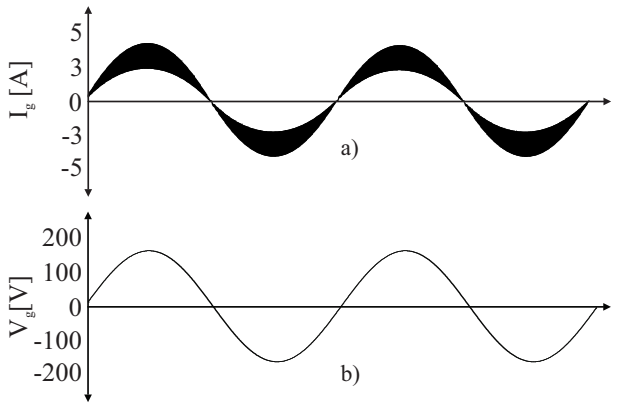

Fig. 16. Simulation result of the system charging a 12S/8.5 Ah battery. (a) Input current waveform. (b) Input voltage waveform.

converters start to operate after charging the dc-bus capacitor, and an optimized control that specifies the dc-bus voltage reference in relation to the load power. The system has some advantages, such as low number of semiconductors, low dc-bus voltage, constant duty cycle, only one current sensor and possibility to galvanic isolate the input source to the battery pack. In addition, by operating the SEPIC PFC rectifier in discontinuous mode, the need for an input filter is reduced.

Lastly, it should be highlighted that this is the first part of the research, and in the following phases, tests will be performed with Lipo batteries and other designs to maximize system optimization.

REFERENCES

[1] P. Daponte, L. D. Vito, G. Mazzilli, F. Picariello, S. Rapuano, M. Riccio, "Metrology for drone and drone for metrology: Measurement systems on small civilian drones", *in Proc. of 2nd IEEE Int. Workshop on Metrology for Aerospace (MetroAeroSpace)*, vol. 1, pp. 306–311, june 2015.

[2] E. Jr, C. Daughtry, C. Walthall, J. III, W. Dulaney, "Agricultural Remote Sensing using Radio-Controlled Model Aircraft", pp. 197–205, jan. 2004, doi: 10.2134/asaspecpub66.c15.

[3] M. N. Boukoberine, Z. Zhou, M. Benbouzid, "Power Supply Architectures for Drones - A Review", *in IECON 2019 - 45th Annual Conference of the IEEE Industrial Electronics Society*, vol. 1, pp. 5826–5831, oct. 2019, doi:10.1109/IECON.2019.8927702.

[4] C. Kyrkou, S. Timotheou, P. Kolios, T. Theocharides, C. Panayiotou, "Drones: Augmenting Our Quality of Life", *IEEE Potentials*, vol. 38, no. 1, pp. 30–36, jan. 2019, doi:10.1109/MPOT.2018.2850386.

[5] M. K. Furrutter, J. Meyer, "Small fuel cell powering an unmanned aerial vehicle", *in AFRICON 2009*, pp. 1–6, sept. 2009, doi:10.1109/AFRCON.2009.5308096.

[6] C. G. Saracin, I. Dragos, A. I. Chirila, "Powering aerial surveillance drones", *in 10th International Symposium on Advanced Topics in Electrical Engineering (ATEE)*, pp. 237–240, mar. 2017, doi:10.1109/ATEE.2017.7905185.

[7] T. Donateo, A. Ficarella, L. Spedicato, A. Arista, M. Ferraro, "A new approach to calculating endurance in electric flight and comparing fuel cells and batteries", *Applied Energy*, vol. 187, pp. 807–819, feb. 2017, doi:10.1016/j.apenergy.2016.11.100.

[8] F.-c. Yang, C.-c. Chen, J.-j. Chen, Y.-s. Hwang, W.-t. Lee, "Hysteresis-Current-Controlled Buck Converter Suitable for Li-Ion Battery Charger", *in International Conference on Communications, Circuits and Systems*, vol. 4, pp. 2723–2726, june 2006, doi:10.1109/ICCCAS.2006.285232.

[9] Y. Ye, C. Chen, J. Jin, L. He, "Li-ion battery management chip for multi-cell battery pack", *in APCCAS 2008 - 2008 IEEE Asia Pacific Conference on Circuits and Systems*, pp. 534–537, nov. 2008, doi: 10.1109/APCCAS.2008.4746078.

[10] S. Bhide, T. Shim, "Development of improved Li-ion battery model incorporating thermal and rate factor effects", *in IEEE Vehicle Power and Propulsion Conference*, pp. 544–550, sept. 2009, doi: 10.1109/VPPC.2009.5289800.

[11] M. Chen, G. A. Rincon-Mora, "Accurate, Compact, and Power-Efficient Li-Ion Battery Charger Circuit", *IEEE Transactions on Circuits and Systems II: Express Briefs*, vol. 53, no. 11, pp. 1180–1184, nov. 2006, doi: 10.1109/TCSII.2006.883220.

[12] L.-R. Dung, C.-E. Chen, H.-F. Yuan, "A robust, intelligent CC-CV fast charger for aging lithium batteries", *in IEEE 25th International Symposium on Industrial Electronics (ISIE)*, pp. 268–273, june 2016, doi:10.1109/ISIE.2016.7744901.

[13] Z. Li, H. Wang, "Comparative analysis of high step-down ratio isolated DC/DC topologies in PEV applications", *in IEEE Applied Power Electronics Conference and Exposition (APEC)*, pp. 1329–1335, mar. 2016, doi:10.1109/APEC.2016.7468040.

[14] D. Wei, F. Darie, H. Wang, "Neighborhood-level collaborative fair charging scheme for electric vehicles", *in ISGT 2014*, pp. 1–5, feb. 2014, doi: 10.1109/ISGT.2014.6816424.

[15] C.-S. Lee, J.-B. Jeong, B.-H. Lee, J. Hur, "Study on 1.5 kW battery chargers for neighborhood electric vehicles", *in IEEE Vehicle Power and Propulsion Conference*, pp. 1–4, sept. 2011, doi: 10.1109/VPPC.2011.6043129.

[16] M. M. U. Alam, W. Eberle, F. Musavi, "A hybrid resonant bridgeless AC-DC power factor correction converter for off-road and neighborhood electric vehicle battery charging", *in IEEE Applied Power Electronics Conference and Exposition - APEC 2014*, pp. 1641–1647, mar. 2014, doi: 10.1109/APEC.2014.6803526.

[17] C. Jung, "Power Up with 800-V Systems: The benefits of upgrading voltage power for battery-electric passenger vehicles", *IEEE Electrification Magazine*, vol. 5, no. 1, pp. 53–58, mar. 2017, doi: 10.1109/MELE.2016.2644560.

[18] C.-Y. Hung, J.-C. Wu, Y.-L. Chen, H.-L. Jou, "A grid-connected battery charger with power factor correction", *in IEEE 11th Conference on Industrial Electronics and Applications (ICIEA)*, pp. 1446–1452, june 2016, doi:10.1109/ICIEA.2016.7603813.

[19] C.-Y. Oh, D.-H. Kim, D.-G. Woo, W.-Y. Sung, Y.-S. Kim, B.-K. Lee, "A High-Efficient Nonisolated Single-Stage On-Board Battery Charger for Electric Vehicles", *IEEE Transactions on Power Electronics*, vol. 28, no. 12, pp. 5746–5757, dec. 2013, doi: 10.1109/TPEL.2013.2252200.

[20] G. Tibola, *Isolated three-phase high power factor rectifier based on the SEPIC converter operating in discontinuous conduction mode*, Ph.D. thesis, Federal University of Santa Catarina, Florianopolis, Brazil, 2013.

[21] H. Suryoatmojo, "Design Li-Po Battery Charger with Buck Converter under Partially CC-CV Method", *in International Seminar on Intelligent Technology and Its Applications (ISITIA)*, pp. 101–106, july 2020, doi: 10.1109/ISITIA49792.2020.9163754.

[22] M. S. Sunita, B. S. Rakshitha, K. Sankirthana, S. Tantry, "A high efficiency, fast response buck converter for low voltage applications", *in IEEE Asia Pacific Conference on Postgraduate Research in Microelectronics and Electronics (PrimeAsia)*, pp. 13–16, nov. 2019, doi: 10.1109/PrimeAsia47521.2019.8950697.

[23] E. H. Ismail, "Bridgeless SEPIC Rectifier With Unity Power Factor and Reduced Conduction Losses", *IEEE Transactions on Industrial Electronics*, vol. 56, no. 4, pp. 1147–1157, oct. 2008, doi: 10.1109/TIE.2008.2007552.

[24] D. Simonetti, J. Sebastian, J. Uceda, "The discontinuous conduction mode Sepic and Cuk power factor preregulators: analysis and design", *IEEE Transactions on Industrial Electronics*, vol. 44, no. 5, pp. 630–637, oct. 1997, doi:10.1109/41.633459.

BIOGRAPHIES

Rafael H. Eckstein, born in Marechal Cândido Rondon, Paraná, Brazil, in 1990, received the B.Sc. and M.Sc. degrees in electrical engineering from Federal University of Santa Catarina (UFSC), Florianópolis, Brazil, in 2012, 2014, respectively. Currently, he is a doctoral student at the Power Electronics Institute (INEP), UFSC. His interests include battery charges and RPAS (Remotely Piloted Aircraft Systems) power systems.

Eduardo Valmir de Souza, was born in Florianópolis, Brazil, in 1982. He received B.S., M.S. and Doctor degrees in electrical engineering from the Federal Usiversity of Santa Catarina (UFSC), Florianópolis, Brazil, in 2007, 2010 and 2015, respectively.

Maikel F. Menke, born in 1989, in Três de Maio - RS. He received the B.S., M.Sc., and Ph.D. degrees in electrical engineering from the Federal University of Santa Maria (UFSM), Santa Maria, Brazil, in 2015, 2016, and 2021, respectively. His research interests include lighting applications, resonant converters, and self-oscillating converters. Dr. Menke is member of the SOBRAEP, and IEEE.

Telles B. Lazzarin, was born in Criciúma, Santa Catarina State, Brazil, in 1979. He received the B.Sc., M.Sc. and Ph.D. degrees in Electrical Engineering from the Federal University of Santa Catarina (UFSC), Florianópolis, Brazil, in 2004, 2006 and 2010, respectively. He is currently an Adjunct Professor at the Department of Electrical and Electronic Engineering (EEL) from the UFSC,and he also works as a Researcher at the Power Electronics Institute (INEP), UFSC.

His interests include switched-capacitor converters, inverters, parallel operation of inverters, high-voltage dc-dc converters, ac-ac power converters and conversion systems for small wind turbines. Dr Lazzarin is a member of the Brazilian Power Electronic Society (SOBRAEP), IEEE Power Electronics Society (PELS) and IEEE Industrial Electronics Society (IES).